

VISUALIZATION OF LIQUID METAL, ARC, AND JET INTERACTIONS IN PLASMA CUTTING OF STEEL SHEET

Byron L. Bemis Gary S. Settles

Keywords: *plasma dynamics, flow visualization, molten metals, metal cutting and fabrication, thermal cutting, ultraviolet imaging, schlieren imaging*

Abstract

This research concerns the fluid- and plasma-dynamic mechanisms involved in plasma cutting, the first step of which is flow visualization. No previous visualization of the plasma cutting front is known, since it is small, extremely hot, and blindingly bright. Experiments were carried out to image oxygen-plasma cutting of 11-gauge mild steel plate with a 30 Amp plasma torch. After solving some key problems of magnification and illumination, it was observed that dross-free cuts result from a stable expulsion of molten ejecta from the plasma cutting front. High-speed dross was seen to arise from a highly-constrained cutting front combined with the wetting of the kerf edges by the melt. Low-speed dross presented the most complex behavior of all, being a chaotic phenomenon subject to flow bifurcations leading to several metastable states of equilibrium. In most of these states, molten ejecta is pumped to the sides of the cutting front by surface tension forces, where it wets the kerf edges, forming dross. In addition to direct imaging, UV and schlieren imaging were also used to shed light on the process.

1 Introduction

It may well be claimed, even in this age of information, that the fabrication of steel structures still drives the industrial world. Steel sheet is cut and welded together to make everything from ships and buildings to automobiles and appliances. The intricate cuts needed for these purposes were traditionally done by oxy-fuel torches, and are sometimes now done by powerful lasers. A third approach, plasma-arc cutting, has grown steadily for decades, and now occupies a significant worldwide role in steel fabrication.

A transferred-arc plasma torch cuts metal plate by first striking an electrical arc between a cathode, located inside the torch, and the metal itself, which forms the anode. A gas (presently oxygen), passed through this arc and constricted through a nozzle, forms a superheated, ionized plasma jet. With temperatures up to 20,000 K, this plasma jet can vaporize most materials. It slices handily through steel plate, ejecting a molten stream of iron and ferrous oxides. The plasma jet thus provides both the thermal energy to melt the metal and the kinetic energy to remove the molten metal from the kerf.

Under optimum conditions the plasma jet produces a clean, narrow kerf through the steel, yielding square, uniform cut edges which require no further finishing step in the manufacturing process (Figure 1). However, non-optimum conditions – especially cutting speeds too low or high or small-radius corners – often produce an adherent “dross.” This dross is actually the molten ejecta from the kerf, having stuck to the sides of the cut and solidified in place. It is highly undesirable,

Contact author: *B. L Bemis, G. S Settles*

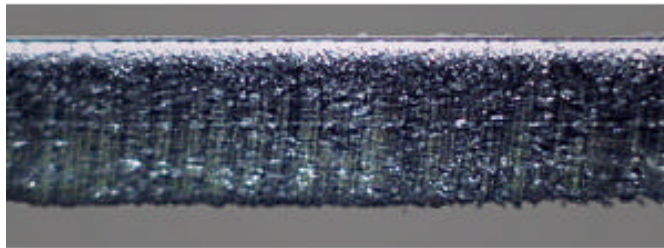
Gas Dynamics Laboratory,

Mechanical Engineering Department

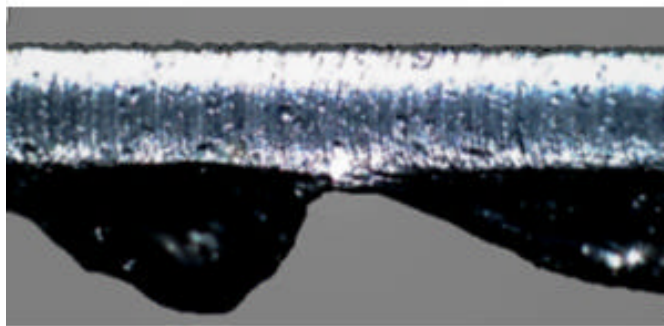
Penn State University

301D Reber Bldg., University Park, PA 16802 USA

since it requires an additional finishing step for removal. This drives the present research to understand the fluid- and plasma-dynamic mechanisms involved in plasma cutting. The first step in achieving this understanding is flow visualization. Little has been published previously on the physics of cutting steel sheet with a plasma torch [1, 2], and notably missing in the prior work is any visualization of the phenomena which occur at the plasma cutting front. This is understandable, however, since the area of interest is small (a few mm in size), extremely hot, and remarkably bright. Our goal in this study is to overcome these obstacles in order to observe the physics of the process. Since the topic is a broad one, present attention is focused chiefly on visualizations to date and what has been learned from them.



Dross Free Plasma Cut Edge



Plasma Cut Edge With Heavy Dross Formation

Figure 1. Typical plasma-cut edges of mild steel sheet (plate thickness = 2.9 mm).

There are three distinct fluid flows involved: 1) the plasma flow, a high-temperature high-speed jet which pierces the workpiece, 2) the shield gas, a cold low-speed gas flow which floods the cut region above the workpiece, primarily to protect the nozzle from molten ejecta during piercing, and 3) the melt flow, produced by the cutting process and driven by the plasma jet. Each of the three flows presents its own challenges for visualization.

2 Experimental Methods

2.1 Plasma Torch

A commercial plasma torch (Hypertherm HyDefinition™ HD-1070 System) with a 30 Amp nozzle was used in these experiments. This equipment produces a highly-constricted oxygen plasma for the purpose of detailed cutting. In all cases described here, 11-gauge cold-rolled AISI-SAE 1008 steel plate (2.9 mm thick) was cut.

In industrial applications the plasma torch is usually mounted on a computer-controlled positioning system, which moves the torch over the workpiece along a desired path, producing the cut. Here, however, for convenience the torch is fixed while the sheet-steel workpiece is translated beneath it via a Velmex stepper-motor drive, as shown in Figure 2. The torch is mounted to a second positioner which allows setting its standoff distance above the workpiece, to which it is oriented perpendicularly. Since the underside of the workpiece is of primary interest for dross formation, the camera viewing angle is typically an oblique upward one from underneath the plate. Even so, several different camera orientations are possible with respect to the direction of the cut.

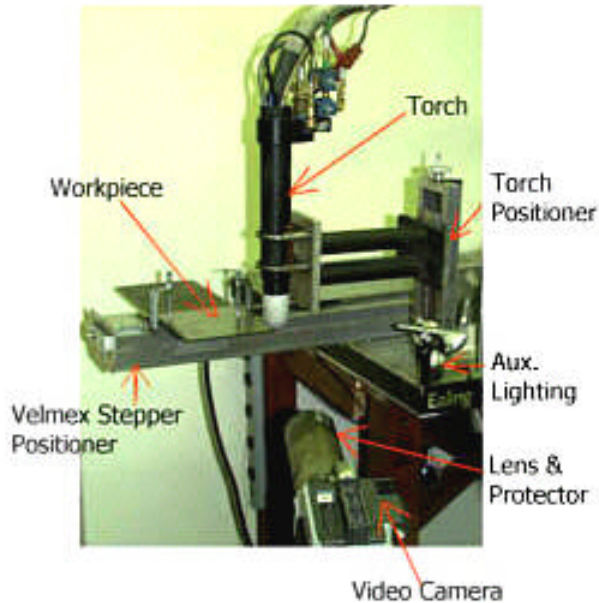


Figure 2. Photo of experimental setup.

2.2 Flow Visualization

2.2.1 Optical Challenges

Difficult problems of image magnification, depth-of-field, and the harsh plasma-cutting environment initially needed solutions in order to visualize the phenomenon of plasma cutting. High magnification presented severe problems in that the immediate region of the cutting front is a harsh environment including high heat, brilliant light emission and molten spatter. Consideration of the actual scale of typical dross nodules, the size of the imager focal plane, and the desired resolution dictated a 4:1 magnification ratio. By mounting a camera lens on an extension tube, this magnification was obtained, according to the thin-lens formulae of geometric optics, with a typical lens standoff distance of 5 cm from the plasma cutting front. However, this put the lens in close proximity to the intense environment of the plasma cut. Further, initial results suffered from a narrow depth-of-focus and “blooming” due to the intense plasma light emission.

A simultaneous solution to these problems was eventually obtained as follows: It is well known

that image depth-of-field increases as the lens aperture is stopped down. This simultaneously reduces the incident light upon the imaging sensor as well. For significant depth-of-field of an intensely-bright subject at extreme magnification, a very small lens aperture is called for. Many camera lenses only stop down to about $f/22$ (lens focal length/unobscured lens diameter = 22), which proved to be insufficient for present purposes. Instead, an auxiliary external lens aperture was used to achieve focal ratios as high as $f/76$, while at the same time protecting the expensive camera lens from damage due to spatter. A sacrificial skylight filter also protected the lens.

While managing the brilliant light emission from the plasma jet, this solution rendered the immediate surroundings of the kerf too dark to see the details of dross solidification and the heat-discolored zone. Auxiliary external illumination of different amounts was thus called for, depending on the camera angle and magnification. Several arrangements were used including multiple lamps and a 650 W focused beam system.

2.2.2 Image Recording

These experiments first employed an S-VHS videocamera fitted with a 50mm focal-length lens and one or two 2X tele-extenders, capped with one of 7 different auxiliary “pinhole” apertures as just described, and shrouded to protect it from damage. With experience, excellent video results were obtained.

However, the standard 30 Hz video frame rate proved insufficient to time-resolve many of the phenomena of plasma cutting. It thus proved necessary to shoot high-speed 16mm films using a Hycam II rotating-prism camera. This approach lacks the instant playback of video, but is far superior in terms of image resolution. The present high-speed movies have the same magnification described previously. 16mm Ektachrome color film having a rating of ISO 160 was used. Cinematography trials determined that a film speed of 1000 frames/sec was sufficient to provide the required temporal resolution of the plasma cutting

and dross formation phenomena under study. This film speed has the effect of slowing the process down by a factor of 42 compared to real-time observation.

Finally, selected still frames were photographed on 35mm color film when high image resolution was required.

2.2.3 Ultraviolet Imaging

Noting that molten iron oxide emits strongly in the ultraviolet, a Schneider UV bandpass filter was interposed in the optical train for some images. This filter blocks wavelengths longer than 405nm and passes the near-UV band between 405nm and the limit of glass transmission at approximately 280nm.

2.2.4 Schlieren Imaging

The mixing and interaction of the plasma jet, shield gas, and atmosphere were observed by a traditional lens-type schlieren system employing a microsecond-flashlamp synchronized with the video camera. A vertical knife-edge cutoff was used to provide the best sensitivity perpendicular to the plasma jet axis. Several different filters and careful masking of the flashlamp image were also used to enhance image contrast despite strong direct light from the plasma jet.

3 Results and Discussion

3.1 Dross Formation

A series of videotapes and high-speed films was obtained which reveal the physical phenomenology of no-dross, low- and high-speed dross formation with high spatial and temporal clarity. The direction of the workpiece motion was either away from or toward the camera, the former orientation giving a clear view of the melt ejection at the bottom leading edge of the kerf and the latter allowing one to see the interior of the leading-edge region and sidewalls. Workpiece motion perpendicular to the camera axis was also used in edge cuts described later. Direct plasma

illumination is not entirely suppressed in these images, but is controlled so as to avoid washing out the details of the kerf and the dross formation.

3.1.1 Dross-Free Cutting

As illustrated in Figure 3, dross-free cuts expel the molten ejecta directly into the plasma jet without wetting the sides of the kerf. This image, looking upward from underneath the workpiece, was shot with metal motion toward the camera's point-of-view. It clearly shows the kerf sides and leading edge, plasma jet, and heat-discolored zone. Even the top kerf leading edge and the torch nozzle are seen. The key observation is that the molten ejecta stream remains ahead of the plasma jet, so that there is no ejecta left to form dross along the kerf edges downstream. More-over, for a range of dross-free cutting speeds this phenomenon shows good stability, recovering from minor perturbations without bifurcating to another flow regime with dross formation. (Note that Figure 3 was taken near the low-speed end of the dross-free cutting regime for present conditions, so it shows an abnormally-wide kerf.)

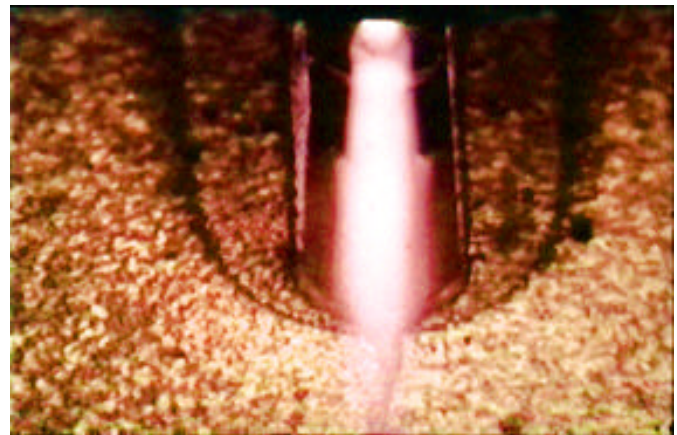


Figure 3. Image of a dross-free plasma cut, viewed from below, trailing the torch.

3.1.2 High-Speed-Dross Formation

Figure 4 illustrates the case of high-speed-dross cutting (typical at cutting speeds above 2.5 cm/sec for present conditions). This image was shot with metal motion away from the camera's point-of-

view, thus emphasizing the kerf bottom leading edge. In contrast with Figure 3, the predominant direction of ejecta flow is clearly to the sides of the cut rather than in front of it. The heat-discolored zone is narrowed and an array of spherical dross nodules is seen to attach to the kerf edges. Also the plasma jet appears shorter and less brilliant than in Figure 3 because a larger fraction of the plasma

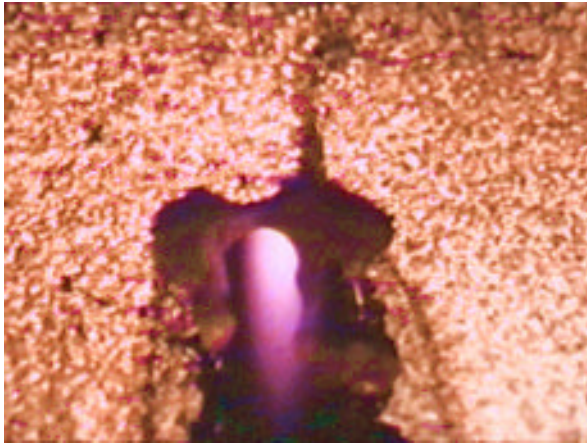


Figure 4. Plasma cut with high-speed dross, viewed from below, leading the torch.

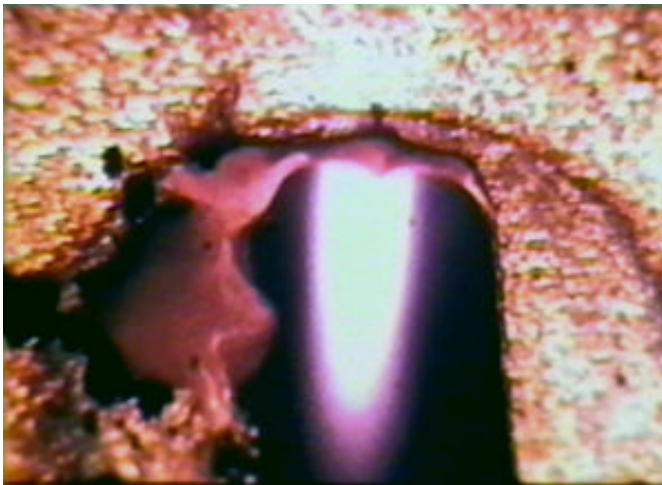


Figure 5. Plasma cut with low-speed dross, viewed from below, leading the torch.

energy has been absorbed by the melt in high-speed cutting. To paraphrase Olsen [3], the major limitation in high-speed plasma cutting is the melt ejection from the narrow kerf leading edge region.

3.1.3 Low-Speed-Dross Formation

In some sense the most interesting case of all is that of low-speed dross (typically at cutting speeds below 1 cm/sec for present conditions). One avoids this regime when possible, but in intricate cuts with corners and small radii it is bound to occur.

As shown in Figure 5, large dross nodules form on the left side of a broad kerf with a similarly-broad heat-discolored zone. Some spattering of small dross nodules ahead of the cut is also apparent. In this example the melt at the right front of the kerf leading edge is actually “pumped” to the left by surface tension forces and possibly the counter-clockwise swirl of the plasma jet core (as viewed from below) induced in the torch for arc stabilization.

Low speed oxygen-based cutting of mild steel is expected to be oxidation-dominated [4]. The cut front temperature is only about 1900 K and the cutting speed is at or below the oxidation rate at this temperature. With an excess of energy available, a wide low-speed kerf and a broad kerf leading-edge region are produced. Exiting from the unconstrained kerf leading-edge region at relatively low speed, the molten ejecta accumulates along the kerf edges, wets these edges, and forms dross nodules.

While Figure 5 shows dross forming only on one side of the kerf, in fact it can occur on either or both sides in practice. Moreover, present observations show that low-speed dross can spontaneously assume a variety of configurations with no obvious natural preference for one over the others. This leads to the view of low-speed dross formation as a chaotic process with nonlinear behavior and sensitive dependence upon both initial and boundary conditions. This is manifested in a variety of metastable states susceptible to flow bifurcations which can shift dross formation from one kerf edge to the other, or cause dross to spontaneously appear or disappear.

Such metastable states are often found in complex nonlinear systems [5]. This detracts from the robustness of the plasma cutting process, since low-speed dross can form in any of a variety of modes which are not readily predictable.

A different view of low-speed plasma cutting with dross formation is seen in the “edge cut” of Figure 6. Here, the edge of the workpiece is traversed through the plasma jet centerline and the camera is aimed perpendicular to the plane defined by the metal edge and this centerline. A unique view of the cutting front and the side of the kerf is thus afforded. This cut was made at a low speed of about 0.6 cm/sec, in which case dross normally forms. However, one must recognize that edge cuts are not normal, since the arc now attaches asymmetrically to the metal.

The formation of curved striations is seen on the cut edge in Figure 6. The gap between the plasma jet and the kerf leading edge is also clearly visible, and is inclined forward at the bottom of the cut, where an interesting glow precedes the plasma jet.

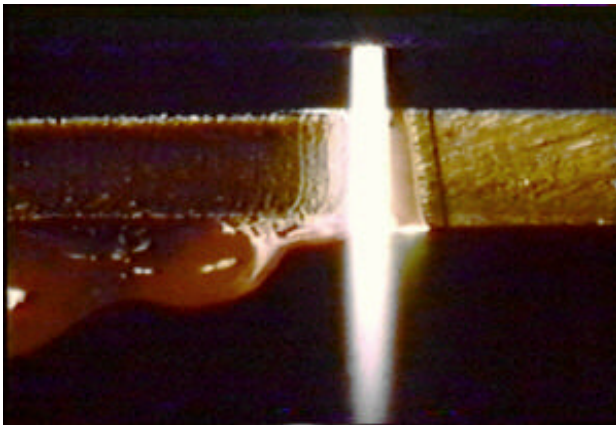


Figure 6. Image of an “edge cut” with low-speed dross formation.

The heat-discolored zone is marked by a dark line parallel to and upstream of the kerf leading edge.

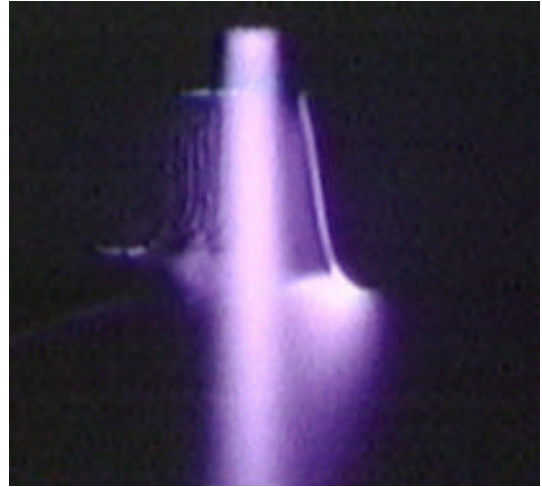


Figure 7. Ultraviolet image of an “edge cut.”

3.2 Ultraviolet Imaging Results

Shown in Figure 7 is the same edge-cut of Figure 6 imaged through the ultraviolet filter described earlier. Most of the UV radiation comes from the plasma jet, with some reflection from the cut edge. However, in the broad gap between the plasma jet and the kerf bottom leading edge is a region of obvious self-luminance. Accumulated evidence suggests strongly that this is the “anode spot,” or point of attachment of the electric arc to the workpiece. A hot-spot of boiling metal at about 3000 K forms at the kerf bottom leading edge, projecting a plume of metal vapor toward the plasma jet. This provides an ionized path for current flow between the anode spot and the cathode inside the torch by way of the plasma jet. UV imaging brings this out clearly due to the strong emission of oxygen and iron ions in the near-UV range.



Figure 8. Ultraviolet image of plasma cutting viewed directly along the plasma jet axis from below the plate.

Another view of this phenomenon is shown in Figure 8, which was taken by way of a small 45° first-surface mirror beneath the workpiece on the plasma jet axis. (The mirror was partially protected by air jets, but was nonetheless regarded as sacrificial.) This view looks directly up the axis of the plasma jet (appearing as a bright circle), with the kerf leading edge on the right. Semicircular UV emission is seen from the kerf leading edge, with a bright anode spot. This image was obtained from a normal, dross-free, 1.9 cm/sec cut, proving that the anode-spot behavior shown previously in Figure 7 is not particular either to abnormal “edge cuts” or to low cutting speeds.

3.3 Schlieren Imaging Results

Two representative schlieren images of the plasma cutting process are shown in Figures 9 and 10. Here the view is from the side, as in Figures 6 and 7, with a fixed torch and workpiece motion from right to left. The bluish background color is due to

the spectrum of the Xenon flashlamp and the optical filtering used here.

Figure 9 reveals that the plasma jet mixes rapidly and turbulently with the surrounding atmosphere underneath the workpiece, as expected in the case of hot jet mixing with cold ambient gas. The turbulence above the workpiece is produced by the shield-gas flow from the torch. At the normal cutting speed represented here, a stream of bright molten ejecta precedes the plasma jet.

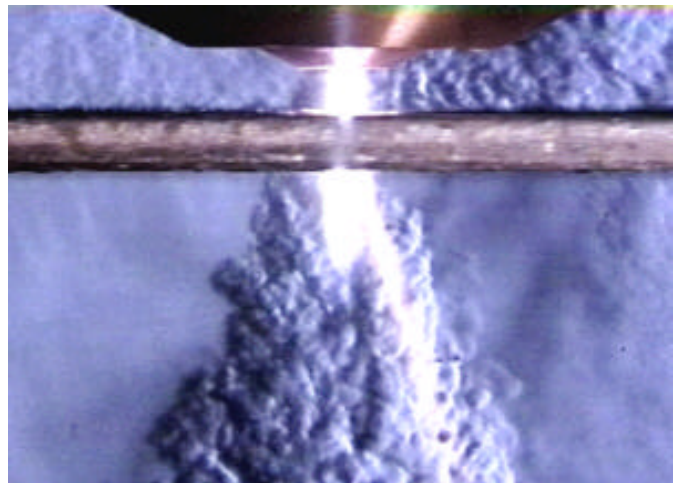


Figure 9. Schlieren image of dross-free plasma cutting.

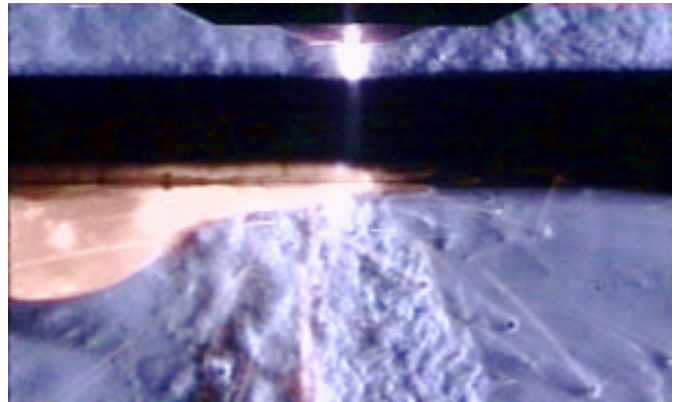


Figure 10. Schlieren image of plasma cutting with low-speed dross.

Figure 10 shows a similar schlieren image at a lower cutting speed, with resulting heavy, glowing dross. No stream of molten ejecta is seen, but forward spatter of small ejecta droplets does occur.

These droplets are observed to have their own thermal trails. Such forward spatter tends to attach to the undersurface of the workpiece ahead of the low-speed cut, where it can subsequently cause a flow bifurcation of the metastable melt ejection pattern described earlier.

3.4 Effect of Workpiece Surface Condition

The sensitivity of low-speed dross to minor changes in boundary conditions is also manifested as a sensitivity to variations in the surface condition of the workpiece. All results shown thus far were for the case of clean steel sheet bearing mill scale. But, to gauge this sensitivity, the mill scale was removed down to bare metal on two sample workpieces, one of which was then corroded for several days in salt water. A third sample was sprayed with boron nitride, used commercially as a non-sticking coating.



Figure 11. Image of a plasma cut with dross formation on a heavily-corroded workpiece, viewed from below leading the torch.

The boron nitride coating inhibited dross formation as expected. On the other hand, bare steel was so readily wetted by the molten ejecta that dross formed at all cutting speeds. The heavily-pitted rusty sample showed intermittent dross formation with an increased tendency for lateral spreading of dross due to surface wetting and irregularities, as illustrated in Figure 11.

4. Observations and Conclusions

The visualization of flows associated with plasma cutting of sheet steel presented some serious initial challenges. Solutions were found to problems of magnification, depth-of-field, illumination, and protection of the camera lens. This allowed direct observation of plasma cutting with high spatial and temporal resolution.

It was then observed that dross-free cuts result from a stable expulsion of molten ejecta from the plasma cutting front. High-speed dross was seen to arise from the incompatibility of a high ejecta flux and a geometrically-constrained cutting front, combined with the wetting of the kerf edges by the melt. Low-speed dross presented the most complex behavior of all, being a chaotic phenomenon subject to flow bifurcations leading to several metastable states of equilibrium. In most of these states, molten ejecta is pumped to the sides of the cutting front by surface tension forces, where it wets the kerf edges, forming dross.

Ultraviolet imaging revealed that the electric arc attaches at the kerf bottom leading edge (under conditions tested here), where an “anode spot” forms and radiates strongly in the UV due to oxygen and Iron ions. The technique of “edge-cutting,” was shown to be effective in revealing this and other phenomena normally hidden inside the kerf. Anode spot behavior was observed both in edge cuts and by the novel approach of imaging directly on the plasma jet axis.

Schlieren imaging was used to reveal the flows associated with the shield gas and the rapid mixing of the plasma jet with the atmosphere underneath the workpiece. Finally, the condition of the bottom surface of the workpiece was shown to play a role in dross formation.

5 Acknowledgments

This research was supported by Hypertherm, Inc. We thank R. W. Couch Jr., C. M. Hackett, and Z-P. Lu, R. C. Dean, Jr., L. J. Dodson, E. B. Hackett, K. C. Potter, and J. D. Miller for their assistance and contributions.

6 References

- [1] **1.** Manohar M and Snyder JP. "Dross formation during Plasma Arc Cutting of Steels." *Welding Journal*, pp. 45-51, Nov. 1994.
- [2] **2.** Nemchinsky VA. "Liquid Metal Movement during Plasma Arc Cutting," *Welding Journal*, pp. 388s-392s, Dec. 1996.
- [3] **3.** Olsen FO. "Fundamental Mechanisms of Cutting Front Formation in Laser Cutting," SPIE Vol. 2207, pp. 402-413, 1994.
- [4] **4.** Miyamoto I and Maruo H. "The Mechanism of Laser Cutting," *Welding in the World*, Vol. 29, No. 9/10, pp. 283-294, 1991.
- [5] **5.** Gleick J. *Chaos*, Penguin Books, NY, 1988.